

## Grafted polymer chains suppress nanoparticle diffusion in athermal polymer melts

Chia-Chun Lin, Philip J. Griffin, Huikuan Chao, Michael J. A. Hore, Kohji Ohno, Nigel Clarke, Robert A. Riggelman, Karen I. Winey, and Russell J. Composto

Citation: *The Journal of Chemical Physics* **146**, 203332 (2017); doi: 10.1063/1.4982216

View online: <http://dx.doi.org/10.1063/1.4982216>

View Table of Contents: <http://aip.scitation.org/toc/jcp/146/20>

Published by the [American Institute of Physics](#)

---

### Articles you may be interested in

[Polymer and spherical nanoparticle diffusion in nanocomposites](#)

*The Journal of Chemical Physics* **146**, 203331 (2017); 10.1063/1.4981258

[Focus: Structure and dynamics of the interfacial layer in polymer nanocomposites with attractive interactions](#)

*The Journal of Chemical Physics* **146**, 203201 (2017); 10.1063/1.4978504

[Network confinement and heterogeneity slows nanoparticle diffusion in polymer gels](#)

*The Journal of Chemical Physics* **146**, 203318 (2017); 10.1063/1.4978054

[Exploring the broadening and the existence of two glass transitions due to competing interfacial effects in thin, supported polymer films](#)

*The Journal of Chemical Physics* **146**, 203330 (2017); 10.1063/1.4979944

[The relationship between dynamic and pseudo-thermodynamic measures of the glass transition temperature in nanostructured materials](#)

*The Journal of Chemical Physics* **146**, 203316 (2017); 10.1063/1.4977520

[Polymer dynamics under cylindrical confinement featuring a locally repulsive surface: A quasielastic neutron scattering study](#)

*The Journal of Chemical Physics* **146**, 203306 (2017); 10.1063/1.4974836

---



**COMPLETELY  
REDESIGNED!**

**PHYSICS  
TODAY**

*Physics Today* Buyer's Guide  
Search with a purpose.

# Grafted polymer chains suppress nanoparticle diffusion in athermal polymer melts

Chia-Chun Lin,<sup>1,a)</sup> Philip J. Griffin,<sup>1,a)</sup> Huikuan Chao,<sup>2</sup> Michael J. A. Hore,<sup>3</sup> Kohji Ohno,<sup>4</sup> Nigel Clarke,<sup>5</sup> Robert A. Riggelman,<sup>2</sup> Karen I. Winey,<sup>1,b)</sup> and Russell J. Composto<sup>1,b)</sup>

<sup>1</sup>Department of Materials Science and Engineering, University of Pennsylvania, Philadelphia, Pennsylvania 19104, USA

<sup>2</sup>Department of Chemical and Biomolecular Engineering, University of Pennsylvania, Philadelphia, Pennsylvania 19104, USA

<sup>3</sup>Department of Macromolecular Science and Engineering, Case Western Reserve University, Cleveland, Ohio 44106, USA

<sup>4</sup>Institute for Chemical Research, Kyoto University, Uji, Kyoto 611-0011, Japan

<sup>5</sup>Department of Physics, University of Sheffield, Sheffield S3 7RH, United Kingdom

(Received 5 December 2016; accepted 10 April 2017; published online 2 May 2017)

We measure the center-of-mass diffusion of poly(methyl methacrylate) (PMMA)-grafted nanoparticles (NPs) in unentangled to slightly entangled PMMA melts using Rutherford backscattering spectrometry. These grafted NPs diffuse  $\sim 100$  times slower than predicted by the Stokes-Einstein relation assuming a viscosity equal to bulk PMMA and a hydrodynamic NP size equal to the NP core diameter,  $2R_{\text{core}} = 4.3$  nm. This slow NP diffusion is consistent with an increased effective NP size,  $2R_{\text{eff}} \approx 20$  nm, nominally independent of the range of grafting density and matrix molecular weights explored in this study. Comparing these experimental results to a modified Daoud-Cotton scaling estimate for the brush thickness as well as dynamic mean field simulations of polymer-grafted NPs in athermal polymer melts, we find that  $2R_{\text{eff}}$  is in quantitative agreement with the size of the NP core plus the extended grafted chains. Our results suggest that grafted polymer chains of moderate molecular weight and grafting density may alter the NP diffusion mechanism in polymer melts, primarily by increasing the NP effective size. *Published by AIP Publishing.* [<http://dx.doi.org/10.1063/1.4982216>]

## I. INTRODUCTION

Depending on nanoparticle (NP) characteristics, polymer nanocomposites (PNCs) can exhibit unique properties ranging from tunable plasmonic absorption<sup>1,2</sup> to enhanced electrical conductivity.<sup>3</sup> Improved mechanical properties<sup>4</sup> and flammability<sup>5</sup> have also been achieved by adding NPs that impart strength and limit combustion, respectively, to the host polymer. In addition to adding functionality to polymers, nanoparticle mobility influences fundamental properties of the PNC such as melt flow and viscosity,<sup>6–11</sup> as well as the effectiveness of self-healing materials to limit crack propagation.<sup>12</sup> Therefore, an improved understanding of nanoparticle diffusion in polymer melts is of both technological and fundamental importance.<sup>13</sup>

The Stokes-Einstein (SE) relation describes the diffusion of a sphere in a continuous medium and is given by

$$D_{\text{SE}} = \frac{k_B T}{6\pi\eta R}, \quad (1)$$

where  $D_{\text{SE}}$  is the Stokes-Einstein diffusion coefficient,  $k_B$  is the Boltzmann constant,  $T$  is absolute temperature,  $\eta$  is the viscosity of the medium, and  $R$  is the NP radius.<sup>14</sup> In a dilute polymer solution, the diffusion of large nanoparticles

(e.g., 0.3–2.2  $\mu\text{m}$ ) is found to obey the SE relationship.<sup>15</sup> However, experimental and theoretical studies have shown that the SE relationship underestimates nanoparticle diffusion when the particle and tube diameter are comparable.<sup>6–8,10,16–21</sup> For example, Grabowski and Mukhopadhyay<sup>18</sup> using a modified version of fluctuation correlation spectroscopy reported that the diffusion coefficient ( $D$ ) of gold NPs in poly(butyl methacrylate) melts is  $\sim 200$  times faster than  $D_{\text{SE}}$  when the NP diameter ( $2R = 5$  nm) is similar to the tube diameter  $d_t \approx 6$  nm. In addition, small NPs can reduce the viscosity of polymer melts, acting akin to plasticizers. This reduction of melt viscosity has been attributed to an increase in free volume due to the fast movement of NPs.<sup>7</sup>

For  $2R \ll d_t$ , Brochard Wyart and de Gennes<sup>13</sup> predicted that nanoparticle diffusion will deviate from SE diffusion because the friction experienced by the NP is no longer captured by the bulk viscosity. Other theoretical studies<sup>22</sup> predict that this transition is gradual and SE diffusion is not recovered until  $2R$  is  $\sim 5$ – $10$  times larger than the tube diameter. Recent experiments have shown that hydrodynamic NP diffusion is indeed recovered when  $2R/d_t$  is  $\sim 5$ – $6$  in polymer melts and in semi-dilute entangled DNA solutions.<sup>23,24</sup> Alternatively, Cai *et al.*<sup>6,25</sup> proposed that a hopping mechanism can enhance nanoparticle mobility when  $2R \sim d_t$ .

To test these prevailing theories, the nanoparticles need to remain well-dispersed during the diffusion experiment. One method to control the dispersion and stability of nanoparticles in a polymer matrix is to graft polymer chains to the NP

<sup>a)</sup>C.-C. Lin and P. J. Griffin contributed equally to this work.

<sup>b)</sup>Authors to whom correspondence should be addressed. Electronic addresses: winey@seas.upenn.edu and composito@seas.upenn.edu

surface. Studies show that dispersion in a polymer matrix can be controlled by varying the ratio of the brush to matrix molecular weight ( $P/N$ ).<sup>1,26–28</sup> Hoshino *et al.*<sup>29</sup> investigated the dynamics of polystyrene (PS)-grafted silica nanoparticles (110 nm) in unentangled PS melts using X-ray photon correlation spectroscopy (XPCS) and observed that nanoparticles followed sub-diffusive behavior when the annealing temperature was greater than  $1.25T_g$ , where  $T_g$  is the glass transition of the PS matrix. This sub-diffusive behavior was attributed to the penetration of short matrix chains into the brush. Kandar *et al.*<sup>30</sup> investigated the effect of grafting density on the dynamics of PS-grafted Au nanoparticles ( $2R_{NP} = 2.4$  nm) in PS matrices. Using XPCS, they observed dynamical arrest at moderate grafting density ( $\sigma = 0.4$  chains/nm<sup>2</sup>), whereas at high grafting density ( $\sigma = 2.3$  chains/nm<sup>2</sup>), liquid-like motion was observed. Liu *et al.* recently demonstrated using XPCS that the NP diffusion mechanism of PS-grafted silica NPs in PS melts is strongly dependent on the nanocomposite morphology.<sup>31</sup> These studies all suggest that the diffusion of polymer-grafted NPs is closely connected to the nature of the grafted layer, namely, the dynamics of the grafted polymer chains and the interpenetration between the brush and matrix chains.

We measure the diffusion coefficient of NPs grafted with poly(methyl methacrylate) (PMMA) chains of molecular weight  $N = 16$  or  $21$  kg/mol and varying grafting density ( $\sigma$ ) in unentangled to slightly entangled PMMA melts of varying matrix molecular weight  $P = 4$ – $52$  kg/mol. Using Rutherford backscattering spectrometry (RBS) to measure the NP diffusion coefficient, we find that these NPs diffuse in PMMA melts  $\sim 100$  times slower than predicted according to the Stokes-Einstein relation assuming a viscosity equal to bulk PMMA and a hydrodynamic NP diameter equal to the NP core,  $4.3$  nm. As  $P/N \leq 2.5$ , the NPs remain well dispersed throughout the duration of the diffusion experiment. We demonstrate that this slow NP diffusion is consistent with a significantly larger effective NP size  $2R_{\text{eff}} \approx 20$  nm, nominally independent of grafting density  $\sigma$  and matrix molecular weight  $P$  in this study. Upon comparing these experimentally determined effective NP sizes to a modified Daoud-Cotton scaling estimate for the brush thickness and dynamic mean field simulations of polymer-grafted NPs in athermal polymer melts, we show that  $2R_{\text{eff}}$  agrees quantitatively with the size of the NP core plus the extended grafted chains. Our results suggest that grafted polymer chains of moderate molecular weight and grafting density suppress the mobility of the NP core via an enlargement of the NP effective size rather than through enhanced friction via entanglements between graft and matrix chains.

## II. EXPERIMENTAL

### A. Materials

Poly(methyl methacrylate) (PMMA) was purchased from various commercial sources and used as received. The supplier, stated molecular weight ( $P$ ), polydispersity index (PDI), and calorimetric glass transition temperature ( $T_g$ ) measured on heating at  $10$  K/min using a Q2000 differential scanning calorimeter (TA Instruments) are shown in

TABLE I. PMMA matrix molecular weight ( $P$ ), ratio of  $P$  and PMMA critical molecular weight ( $24$  kg/mol),<sup>33</sup> polydispersity index, calorimetric glass transition temperature, and commercial supplier.

$P$ (kg/mol)	$P/P_c$	PDI	$T_g$ (K)	Supplier
4	0.17	1.1	369	Polymer laboratories
8	0.33	1.1	368	Polymer source
14	0.58	1.09	377	Polymer source
17.5	0.73	1.1	381	Pressure chemical
20	0.83	1.14	390	Polymer source
34	1.42	1.06	393	Polymer laboratories
52	2.17	1.09	397	Pressure chemical

Table I. PMMA-grafted iron oxide nanoparticles (NPs) were synthesized using methods described elsewhere.<sup>32</sup> The NP core diameter is log-normally distributed with a geometric mean particle diameter  $2R_{\text{core}} = 4.3$  nm and standard deviation  $e^\sigma = 1.2$  as determined by image analysis of transmission electron micrographs of polymer nanocomposite thin films. Three sets of PMMA-grafted NPs of varying grafting density and graft molecular weight were studied:  $\sigma = 0.17$  chains/nm<sup>2</sup>,  $N = 21$  kg/mol (0.17-21);  $\sigma = 0.33$  chains/nm<sup>2</sup>,  $N = 21$  kg/mol (0.33-21); and  $\sigma = 0.55$  chains/nm<sup>2</sup>,  $N = 16$  kg/mol (0.55-16).

### B. Diffusion couple sample preparation

For NP diffusion measurements, a series of bilayer samples consisting of thick PMMA matrix films ( $>5$   $\mu\text{m}$ ) topped with thin ( $50$  nm, as measured by ellipsometry) polymer nanocomposite (PNC) films were prepared. For the matrix films, PMMA was dissolved in dimethylacetamide (DMAc), stirred for  $20$  h, and the solution was doctor bladed on a heated ( $120$  °C) glass substrate. After drying, the PMMA matrix film was floated from the glass substrate in water, picked up using a silicon wafer, and annealed for  $3$  days in vacuum at  $T_g + 75$  K. The PNC thin tracer films consisted of PMMA-grafted NPs blended with PMMA of the same molecular weight as the corresponding matrix film. To prepare these PNC films, PMMA and the polymer-grafted NPs were dissolved in toluene in separate vials and stirred for  $20$  h. The necessary amount of NP solution to achieve NP iron oxide-core volume fractions of  $2.5$  vol. % was then mixed with the PMMA solution and stirred for another  $20$  h. The PNC thin films were prepared by spin-coating the PMMA/NP solution onto a silicon wafer previously treated with a water soluble chitosan sacrificial layer. The PNC tracer film was floated off the silicon wafer in water by dissolving the sacrificial layer and then collected onto the PMMA matrix film. These diffusion couples were then annealed in vacuum at  $T_g + 75$  K (cf. Table I) for various annealing times such that the NP diffusion lengths were  $\sim 500$  nm.

### C. Rutherford backscattering spectrometry

Rutherford backscattering spectrometry (RBS) was used to measure the concentration profiles of iron oxide NPs in the diffusion couples, as previously described.<sup>34</sup> In the RBS experiment, helium ions ( $\text{He}^+$ ) of energy  $2.023$  MeV are incident normal to the plane of the diffusion couple sample, and

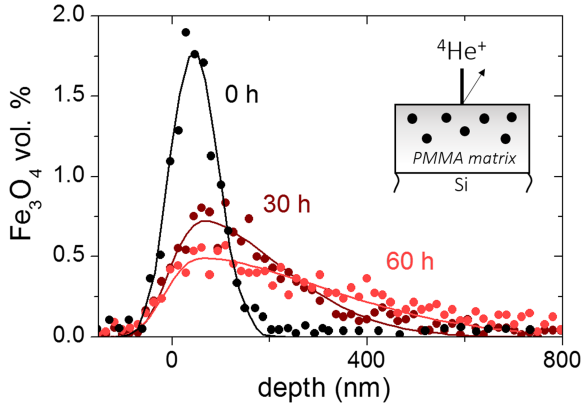


FIG. 1. Concentration profiles of PMMA-grafted iron-oxide nanoparticles (0.33-21) diffused into 52 kg/mol PMMA after annealing at 465 K for 0, 30, and 60 h. Symbols depict measured data, and the solid lines depict fits used to determine the NP diffusion coefficient ( $D = 1.8 \times 10^{-15} \text{ cm}^2/\text{s}$  independent of annealing time). The inset shows a schematic representation of the RBS experiment.

the energy of backscattered  $\text{He}^+$  ions ( $\theta = 170^\circ$ ) is measured using a solid-state detector. Data collection continued until the yield near the maximum NP concentration reached  $\sim 100$  counts, typically an integrated charge of  $\sim 30 \mu\text{C}$ . The RBS yield versus channel spectra are then converted to NP volume fraction versus depth into the matrix. According to recent theoretical and simulation studies of NP mobility in unentangled and entangled polymer melts, the long time and length scale motion of NPs is diffusive.<sup>6,19,22</sup> As such, we have chosen to analyze our measured concentration profiles (which span very long time and length scales) using the Fickian diffusion model, which captures well the NP concentration profiles, Fig. 1. It should be noted, however, that XPCS studies of NP diffusion in well entangled polymer melts have revealed anomalous, hyper-diffusive NP motion (cf. Ref. 20). Resolving this discrepancy is an important task but outside the scope of our current study. The NP diffusion coefficient was obtained by fitting the concentration profile using the one-dimensional solution of Fick's second law for a finite source in a semi-infinite medium,

$$\phi(x) = \frac{1}{2} \left[ \text{erf} \left( \frac{h-x}{\sqrt{4Dt}} \right) + \text{erf} \left( \frac{h+x}{\sqrt{4Dt}} \right) \right], \quad (2)$$

where  $x$  is depth,  $h$  is the PNC tracer film thickness,  $t$  is annealing time, and  $D$  is the diffusion coefficient. Experimental depth profiles were fit using Eq. (2) convoluted with the Gaussian instrumental resolution function (half width = 35 nm), and the accessible depth was  $\sim 800$  nm.

#### D. Three-dimensional dynamic mean field simulations

We employ a coarse-grained molecular model for our polymer nanocomposite system. Both the matrix and grafted PMMA polymers in the experiment are modeled as discrete Gaussian chains where the chain connectivity is maintained by harmonic bonds. One end of the grafted chains is bonded to an anchor point that is fixed on the NP surface. The total bonded potential is the summation over the elastic energy stored in the harmonic bonds,

$$\frac{U_b}{k_B T} = \sum_{i=1}^{n_P} \sum_{j=1}^{P-1} \frac{3(r_{i,j} - r_{i,j+1})^2}{2b^2} + \sum_{i=1}^{n_N} \sum_{j=1}^{N-1} \frac{3(r_{i,j} - r_{i,j+1})^2}{2b^2} + \sum_{i=1}^{n_N} \frac{3(r_{i,N} - r_{g,i})^2}{2b^2}, \quad (3)$$

where  $N$  and  $P$  denote the number of segments in the grafted and matrix chains while  $n_N$  and  $n_P$  denote the number of grafted and matrix chains, respectively. Here,  $b$  is the statistical segment length;  $r_{g,i}$  is the location of the anchor point on the NP surface bonding the last segment in  $i$ th grafted chain to the NP. These anchor points are randomly distributed on the NP surface and move as a rigid body as the NP rotates.

Non-bonded interactions are taken through a Helfand compressibility potential<sup>35</sup> that penalizes deviations of the local total density  $\tilde{\rho}_+(\mathbf{r})$  from the average density  $\rho_0$

$$\beta U_{nb} = \frac{\kappa}{\rho_0} \int d\mathbf{r} \left[ \tilde{\rho}_+(\mathbf{r}) - \rho_0 \right]^2, \quad (4)$$

where  $\kappa$  controls the compressibility of the system. The density of each component, the polymer monomers and the nanoparticle core, is given by a shape function that describes the distribution of the mass about the component's center. For the polymer monomers, we use a unit Gaussian  $h(\mathbf{r}) = \left( \frac{1}{2\pi a^2} \right)^{\frac{3}{2}} e^{-|\mathbf{r}|^2/2a^2}$ , where  $a$  is a length scale that controls the range of the interaction. For the NP, we employ  $\Gamma(\mathbf{r}) = \frac{\rho_0}{2} \text{erfc} \left( \frac{|\mathbf{r} - \mathbf{r}_{NP}| - R_p}{\xi} \right)$ , which has the form of a spherical step function with radius  $R_p$  that smoothly decays from the bulk density in the center  $\rho_0$  to 0 over a length scale controlled by  $\xi$ . The total density is then given by  $\tilde{\rho}_+(\mathbf{r}) = \sum_i h(\mathbf{r} - \mathbf{r}_i) + \Gamma(\mathbf{r})$ , where the sum over  $i$  goes over all monomers in the system. It can be shown that the effective non-bonded interaction between the different components is given by a convolution of the shape functions,<sup>36,37</sup> which makes the non-bonded interactions non-local. We sample the model using a 3D version of dynamic mean field theory<sup>38</sup> that we have recently implemented,<sup>39</sup> which uses a particle-to-mesh scheme to evaluate the non-bonded interactions and is similar in spirit to single-chain in mean field<sup>40</sup> and related methods.<sup>41</sup> We note that although our implementation involves a dynamic mean-field approximation, thermodynamic fluctuations are accurately sampled.<sup>39</sup>

To map our Gaussian chain models onto the experimental PMMA polymers, we set up the number of segments in the Gaussian chain,  $N_{CG}$ , and the statistical segment length,  $b$ , such that the unperturbed radius of gyration of the Gaussian chain,  $R_g = \sqrt{\frac{N_{CG}-1}{6}} b$ , matches the radius of gyrations of the real PMMA polymer,  $R_{g,exp} = \sqrt{\frac{n-1}{6}} b_{exp}$ , where  $n$  is the number of monomers and  $b_{exp}$  is the experimentally measured statistic segment length in the real PMMA polymer. By adopting the experimentally measured  $b_{exp}$  for PMMA at 0.66 nm<sup>33</sup> and choosing  $b$  at 1.96 nm, the grafted PMMA polymers with molecular weight, 16 and 21 kg/mol, are mapped to the Gaussian chains with  $N$  of 18 and 24 monomers, respectively. At the same time, the matrix PMMA polymers with molecular weight 4, 14, and 52 kg/mol are mapped to the Gaussian chains with  $P$  of 4, 16, and 60 monomers, respectively. To ensure the Gaussian chain has

the same volume as for the real PMMA polymer, we use the equation,  $v = \frac{n}{N_{CG}} v_{exp}$ , to determine the monomer volume,  $v$ , in the Gaussian chain and the average density,  $\rho_0 = v^{-1}$ . Here, the experimentally measured PMMA monomer volume,  $v_{exp} = 0.149 \text{ nm}^3$ .<sup>33</sup>

In the simulations, all the dimensional quantities are scaled by the statistical segment length,  $b$ , and the energy unit is set to  $k_b T$ . The temporal quantities used here are normalized by the segment diffusion time  $b^2/D_0$ , where  $D_0$  is the segment diffusion coefficient used in the Langevin equation. We employ a compressibility  $\kappa = 140$  to suppress large density deviations from the bulk value. The spatial resolution is  $dx = 0.25$ , and the time step is  $\delta t = 0.02$ . The NP interfacial width,  $\xi = 0.25$  and the segment smearing size,  $a$ , are approximated as  $a = \frac{b}{2}$ . Each simulation ran for approximately two million iterations after the equilibration stage and trajectories were saved every  $10^3$  iterations to calculate the chain volume fraction profiles about the NP. Possible error sources in the dynamic mean field simulations include the discretization of the Gaussian chain with finite number of segments  $N_{CG}$  to model the PMMA polymers. To test this, we have doubled  $N_{CG}$  by decreasing  $b$  for selected designs of the simulation system and found no appreciable changes in the corresponding density profiles of the grafted chains.

We compare these 3D dynamic mean field volume fraction profiles to 2D self-consistent field theory calculations in the [supplementary material](#), Fig. SI. 1. There are clear quantitative differences between the volume fraction profiles determined by these different techniques, although qualitatively, they show similar trends. We attribute these differences to the relative importance of thermodynamic fluctuations at such short chain lengths, as well as the important difference in packing of grafted polymer chains in two (cylindrical) versus three (spherical) dimensions.

### III. RESULTS AND DISCUSSION

Figure 2 shows representative transmission electron micrographs of the PNC tracer films across the range of studied ratios of matrix to graft molecular weight ( $P/N$ ) and PMMA grafting densities. For all grafting densities, the NPs are

well-dispersed in the PMMA matrix up to  $P/N \sim 2.5$ , beyond which NPs aggregated presumably due to depletion-attraction forces.<sup>27</sup> This result is consistent with the wet to dry brush transition reported in literature.<sup>1,26-28</sup> To confirm that NPs remain well-dispersed during annealing of the diffusion couples, we have used RBS to analyze the NP concentration profiles of all samples at multiple annealing times (Fig. 1). We interpret the observed annealing time-independent NP diffusion coefficients as evidence that the NPs remain well-dispersed during annealing. If the NPs were to aggregate during annealing, the large increase in effective particle size would result in a diffusion coefficient that decreases dramatically with annealing time. We find annealing time-independent diffusion coefficients for all NP/polymer matrix combinations where  $P/N < 2.5$ , while for systems with  $P/N > 2.5$ , we find from RBS analysis that the NPs aggregate near the surface during annealing and do not diffuse deeply into the PMMA matrix.

The nanoparticle diffusion coefficients decrease with increasing matrix molecular weight and are largely independent of grafting density and graft molecular weight, Fig. 3. We do note, however, that the diffusion coefficients of the 0.55-16 NPs are slightly greater than those of the 0.17-21 and 0.33-21 NPs, a difference that may be attributable to the slightly smaller graft molecular weight (and thus shorter length of the grafted chain). Because our NP diffusion measurements span PMMA matrix molecular weights from well below to moderately above the critical molecular weight ( $\sim 24 \text{ kg/mol}$  for PMMA<sup>33</sup>), we caution against strict interpretation of the observed molecular weight dependence of the measured NP diffusion coefficients or the apparent deviations from Rouse ( $M_w^{-1}$ ) or entanglement ( $M_w^{-3.4}$ ) controlled friction.<sup>42</sup>

We next compare the measured NP diffusion coefficients to those predicted according to the Stokes-Einstein relation (Eq. (1)). Because the NP core volume fraction is very low for these experiments and representative of the dilute limit, we first employ the viscosity of the bulk PMMA (with 0 vol. % NPs) to account for the hydrodynamic friction experienced by these NPs. We have measured the zero-shear viscosity of bulk PMMA at three molecular weights spanning

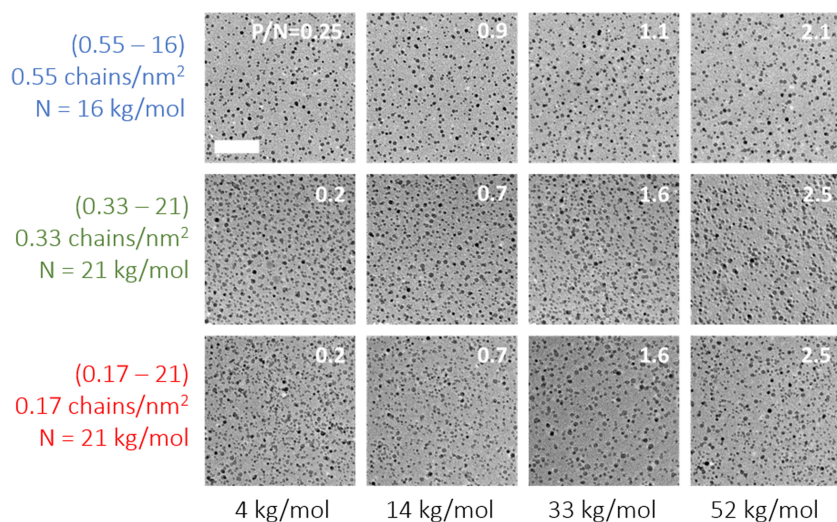


FIG. 2. Top-view transmission electron micrographs of polymer nanocomposite tracer layers ( $\varphi_{NP} = 0.025$ , thickness = 50 nm) across the range of NP type (grafting density, grafting molecular weight,  $N$ ) and matrix molecular weights,  $P$ . The ratio of matrix and graft molecular weight ( $P/N$ ) is shown in the upper-right corner of each micrograph, and the scale bar is 100 nm.

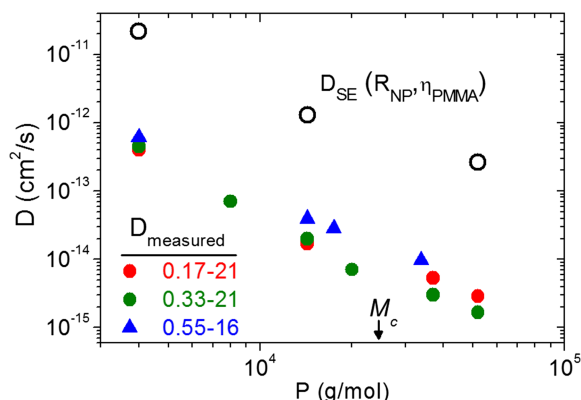


FIG. 3. Nanoparticle diffusion coefficients measured at  $T_g + 75$  K (solid symbols) and predicted according to the Stokes-Einstein relation (open symbols) using the measured viscosity of bulk PMMA and the nanoparticle core radius. The PMMA critical molecular weight is indicated with an arrow.

the range of NP diffusion measurements, and provide direct comparisons at these three values of  $P$  only. As is seen in Fig. 3, the measured NP diffusion coefficients are significantly lower ( $\sim 100$  times) than predicted by the Stokes-Einstein relation across all matrix molecular weights and grafting densities. The observed, excessively slow diffusion of these grafted NPs is quite surprising given that the NP core diameter  $2R_{\text{core}} = 4.3$  nm is significantly smaller than the tube diameter of PMMA ( $d_{\text{tube}} \approx 6-7$  nm) or the polymer coil size ( $2R_g$ ) for most of the matrix molecular weights studied herein.

Theoretical studies have predicted and experiments have shown that apparent faster-than-Stokes-Einstein NP diffusion may occur when the NP diameter is smaller than these characteristic length scales in entangled polymer melts because chain-scale friction no longer controls the mechanism of nanoparticle diffusion.<sup>6-8,10,16-19</sup> These predictions are strictly valid only for bare nanoparticles exhibiting neutral interactions with the polymer matrix, and the NP diffusion experiments available in literature have primarily focused on similar cases. Recently, Mangal *et al.* measured the mobility of polymer-grafted NPs in polymer melts using X-ray photon correlation spectroscopy, finding faster-than-Stokes-Einstein diffusion of PEO-grafted NPs in entangled PMMA melts.<sup>20</sup> It should be noted, however, that the graft molecular weight in these studies was quite small (2 kg/mol), while in our studies the graft molecular weights are 16 or 21 kg/mol. This larger graft molecular weight may considerably augment the effective hydrodynamic NP size and contribute to the observed slow NP diffusion. In this regard, the current data may reflect a similar case as our recent studies of the diffusion of silica NPs in poly(2-vinyl pyridine) melts,<sup>23</sup> where we found unexpectedly slow NP diffusion consistent with the formation of a polymer bound layer that increases the effective NP hydrodynamic size.

To account for these dramatically lower-than-expected NP diffusion coefficients, we begin by assuming that the NPs diffuse with an unknown and significantly augmented effective diameter  $2R_{\text{eff}}$ , and the Stokes-Einstein relation in fact holds when describing the diffusion of these presumably larger grafted-NPs. This assumption is reasonable in light of the fact that most of our experiments explore diffusion of NPs

in the unentangled regime where the SE relation is expected to be valid.<sup>22</sup> We do not expect this assumption to hold in highly entangled polymer melts unless the particles are much larger than the tube diameter ( $2R/d_t > 5-6$ ).<sup>22,23</sup> We rewrite the Stokes-Einstein relation describing the measured NP diffusion as

$$D = \frac{k_B T}{6\pi\eta_{\text{PNC}}R_{\text{eff}}}, \quad (5)$$

which accounts for the new effective NP diameter  $2R_{\text{eff}}$  and the correspondingly larger zero-shear viscosity of the PNC  $\eta_{\text{PNC}}$ . We estimate the viscosity of the PNC by assuming that the effective nanoparticles interact as hard spheres and enhance the viscosity of the polymer melt in a manner similar to colloidal suspensions.<sup>43</sup> In our current case, the measured NP diffusion coefficients are  $\sim 100$  times slower than predicted by the SE relation for the NP core in a PMMA melt, which suggests that the effective NP diameter is many times larger than  $2R_{\text{core}}$ . It is thus possible that the effective NP volume fraction  $\varphi_{\text{eff}} = \varphi_{\text{core}} \left(\frac{R_{\text{eff}}}{R_{\text{core}}}\right)^3$  is quite large and may be approaching the random close packed jamming volume fraction  $\varphi_{\text{max}} \approx 0.63$ .

At these potentially large effective volume fractions, it has been shown that the zero-shear viscosities of colloidal suspensions<sup>44</sup> and highly loaded polymer nanocomposites<sup>45</sup> are no longer well-described by Einstein's equation (corrected to second order), but rather follows well the phenomenological Krieger-Dougherty equation,<sup>46,47</sup>

$$\eta_{\text{PNC}} = \eta_{\text{poly}} \left(1 - \frac{\varphi_{\text{eff}}}{\varphi_{\text{max}}}\right)^{-2}. \quad (6)$$

We use this relation to estimate the PNC viscosity and write the normalized diffusion coefficient,

$$\frac{D}{D_{\text{SE}}} = \frac{R_{\text{core}} \cdot \eta_{\text{poly}}}{R_{\text{eff}} \cdot \eta_{\text{PNC}}} = \frac{R_{\text{core}}}{R_{\text{eff}}} \left(1 - \frac{\varphi_{\text{core}}}{\varphi_{\text{max}}} \left(\frac{R_{\text{eff}}}{R_{\text{core}}}\right)^3\right)^2, \quad (7)$$

where  $D$  is the measured diffusion coefficient (described by Eq. (5)) and  $D_{\text{SE}}$  is the SE relation describing the diffusion of the NP core in the neat PMMA melt. The NP-core volume fraction varies from  $\sim 0.0025$  to  $0.0075$  with an average  $\varphi_{\text{core}} \approx 0.005$  (see Fig. 1) for all analyzed annealed concentration profiles, and we thus solve Eq. (7) to determine  $R_{\text{eff}}$  at  $\varphi_{\text{core}} = 0.005$  for all measured ratios  $D/D_{\text{SE}}$ , Fig. 4(a). We have also calculated  $R_{\text{eff}}$  at  $\varphi_{\text{core}} = 0.0025$  and  $0.0075$  for the 0.17-21 NPs and include this information as error bars in Fig. 4(a).

Figure 4(a) shows the effective NP diameter  $2R_{\text{eff}}$  determined from Eq. (7) for the three grafted NPs as a function of matrix molecular weight. The effective NP diameter  $2R_{\text{eff}} \approx 18-20$  nm is more than four times larger than the NP core diameter  $2R_{\text{core}}$  and is essentially independent of the grafting densities and matrix molecular weights used here. Furthermore, this effective NP size is nearly 3 times larger than the tube diameter of PMMA, where at the studied unentangled-to-weakly entangled matrix molecular weights, significant deviations from hydrodynamic NP diffusion are not predicted.<sup>22</sup> As shown in Fig. 4(b), these larger effective NPs increase the matrix viscosity due to the larger effective NP volume fractions (we find  $\varphi_{\text{eff}} \sim 0.40-0.50$  for the studied cases).

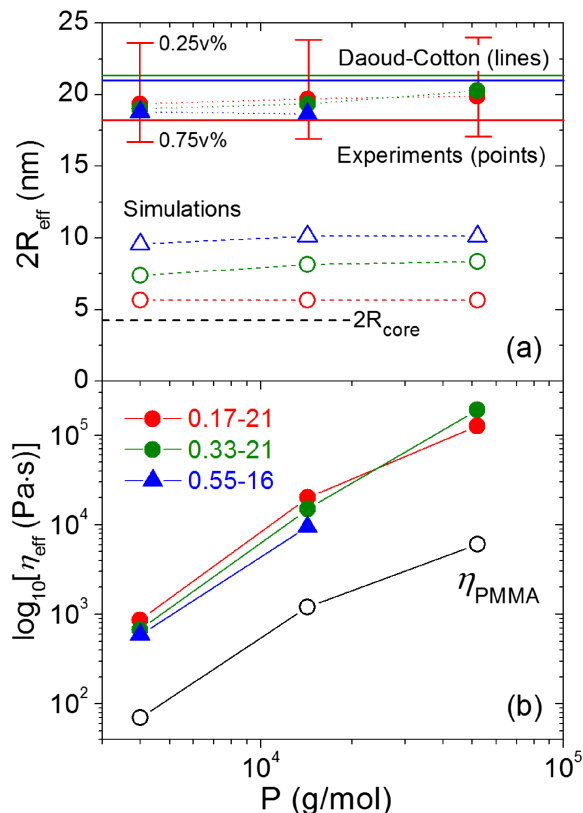


FIG. 4. (a) Effective nanoparticle diameter in the melt as determined by NP diffusion measurements (solid symbols), the modified Daoud-Cotton scaling approach (solid lines), and dynamic mean field simulations (open symbols) plotted as a function of matrix molecular weight. Upper and lower error bars on experimental data correspond to  $R_{\text{eff}}$  values of the 0.17-21 NPs calculated at  $\varphi_{\text{core}} = 0.0025$  and  $0.0075$ , respectively (as described in text).  $R_{\text{eff}}$  from simulations is determined as the distance from the NP center to where matrix chains occupy exactly 50% of the total volume. (b) The calculated effective zero-shear viscosity of the nanoparticle-modified PMMA melt (solid symbols), as well as the measured zero-shear viscosity of bulk PMMA (open symbols).

The presence of grafted polymer chains at the moderate molecular weights and grafting densities studied herein likely augments the effective hydrodynamic size of these small-core NPs. Using a modified Daoud-Cotton model, Ohno *et al.* quantified the brush height of PMMA-grafted silica NPs (of moderate grafting density with a broad range of graft molecular weights) in good solvent.<sup>48,49</sup> More recently, Hore *et al.* used small angle neutron scattering to test the validity of the model for describing the brush thickness of PMMA-grafted iron oxide NPs suspended in PMMA melts and found good agreement.<sup>50</sup> In the concentrated polymer brush regime, the brush thickness  $h$  is well described by this modified Daoud-Cotton model such that

$$h \left( 1 + \frac{h}{2R_{\text{core}}} \right) = a (\sigma s_m)^{1/2} l_m N, \quad (8)$$

where  $a$  is a constant of order one,  $\sigma$  is the graft density,  $s_m$  is the cross-sectional area of the graft chain,  $l_m$  is the contour length per monomer, and  $N$  is the graft degree-of-polymerization. Using the same parameters for PMMA-grafted chains as in the study of Ohno *et al.* ( $a = 1.15$ ,  $s_m = 0.54 \text{ nm}^2$ ,  $l_m = 0.25 \text{ nm}$ ), we have estimated the brush thickness for the three PMMA-grafted NP systems studied

herein and plot the corresponding effective NP diameter along with the experimental data in Fig. 4(a). As seen in Fig. 4(a), these Daoud-Cotton estimates agree well with the experimentally determined effective NP sizes, suggesting that NP mobility in these studied systems is well-approximated by the SE relation and furthermore the effective hydrodynamic NP size is determined by the full radial extent of the grafted polymer chains.

We have also employed dynamic mean field simulations to model our experimental systems and provide a more detailed understanding of the structure of the grafted polymer layer on these NPs. We have simulated a grafted nanoparticle (at three grafting densities corresponding to the three experimental systems) dispersed in an athermal polymer matrix corresponding to the PMMA molecular weights for which we have measured viscosity data. From these simulations, we have calculated the 3-dimensional graft and matrix chain volume fraction profiles averaged over the polar and azimuthal angles. Figure 5(a) presents these averaged volume fraction profiles for the 0.33-21 grafted NP embedded in an athermal polymer melt of molecular weight  $P = 4, 14$ , and  $52 \text{ kg/mol}$ . The grafted polymer layer is strongly wet by the matrix chains as indicated by the relatively high matrix volume fraction near the NP core surface,  $R_{\text{core}} = 2.15 \text{ nm}$ . The grafted polymer chains also occupy a substantial part of the total volume out to distances several times larger than  $R_{\text{core}}$ . Furthermore, the

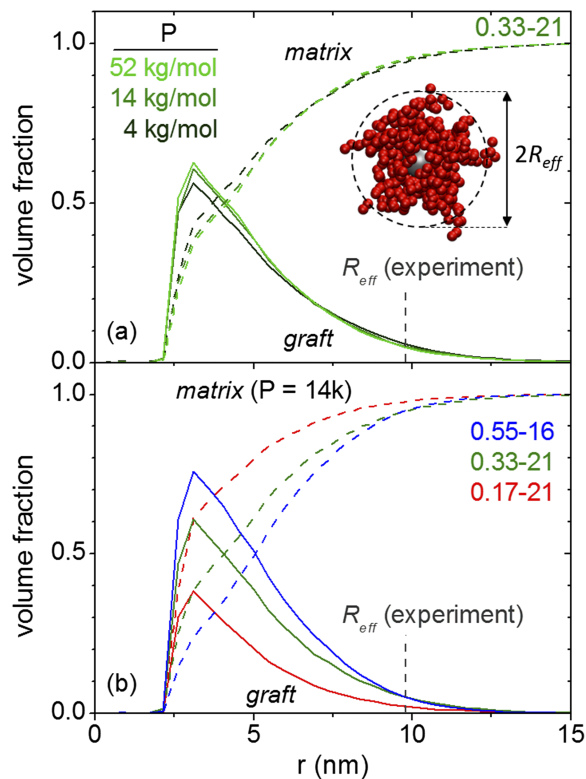


FIG. 5. Volume fraction profiles of grafted (solid line) and matrix (dashed line) polymer chains calculated from 3D dynamic mean field simulations. (a) NPs with grafting density  $0.33 \text{ chains/nm}^2$  and graft molecular weight  $21 \text{ kg/mol}$  (0.33-21) suspended in a polymer melt of varying molecular weight (4, 14, and  $52 \text{ kg/mol}$ ). (b) NPs of varying grafting density suspended in the  $14 \text{ kg/mol}$  matrix. Inset: simulation snapshot of the 0.33-21 grafted NP in the  $14 \text{ kg/mol}$  melt, where the dashed circle depicts the effective hard sphere particle size determined from NP diffusion measurements.

graft volume fraction profiles are nearly independent of matrix molecular weight for all studied systems. These aspects of the simulations corroborate two key observations in our experimental data—namely, the large effective NP size and its weak dependence on matrix molecular weight (Fig. 4(a)).

Consistent with our previous studies,<sup>51</sup> we estimate the simulated effective NP radius as the distance from the NP center where the matrix chains occupy exactly 50% of the total volume. As seen in Fig. 5(a), this distance is relatively close to the surface of the NP core, around  $r \approx 4$  nm. We plot this volume-fraction estimation of  $2R_{\text{eff}}$  along with the experimental data in Fig. 4(a). At fixed grafting density and graft molecular weight, these effective sizes determined from the simulations are essentially independent of matrix molecular weight, consistent with the experimental results. At fixed  $P$ , the simulated effective NP size increases by nearly a factor of two as grafting density increases from 0.17 to 0.55 chains/nm<sup>2</sup>. This result stands in contrast with the experimental data, where it is seen that  $2R_{\text{eff}}$  determined experimentally is essentially independent of grafting density and is several times larger than this volume-fraction estimation of the effective NP size.

Alternatively, we consider the thickness of the grafted polymer layer as defined by the maximum radial extent of the grafted polymer chains, a quantity that is directly connected to the modified Daoud-Cotton estimate of the polymer brush thickness. It is seen in Fig. 5(a) that the graft volume fraction profiles exhibit similar radial dependencies regardless of matrix molecular weight at  $r > 6$  nm. Apart from a total decrease in volume fraction with decreasing grafting density, Fig. 5(b) illustrates that the radial dependence is qualitatively independent of grafting density. The maximum extent of the grafted polymer layer is  $r_{\text{max}} \sim 12.5$  nm and nominally independent of NP type (grafting density and grafting molecular weight) and matrix molecular weight. This  $2r_{\text{max}}$  is comparable to the experimentally determined hydrodynamic diameter of these grafted NPs diffusing in PMMA melts (solid symbols, Fig. 4) and the above-mentioned modified Daoud-Cotton estimate for the brush thickness. This agreement indicates that the effective size of polymer grafted nanoparticles in athermal polymer melts is largely controlled by the furthest extent of the grafted chains rather than the degree of exclusion of matrix chains by the grafted chains. Alternatively, our results could also indicate that the grafted chains are significantly slowing the diffusion of matrix chains in their near vicinity, effectively “dragging” them during the slow process of NP diffusion and augmenting the effective NP size in this manner. Either way, these results clearly show that polymer grafts of moderate molecular weight and grafting density dramatically alter the diffusion mechanism of NPs in unentangled to lightly entangled athermal polymer melts. Moreover, this study has established a robust experimental and theoretical approach to exploring grafted NP diffusion that can be expanded to a wider variety of systems. Finally, we would like to emphasize that the findings of this study may be limited to the range of currently explored experimental parameters (namely, grafting densities and molecular weight), and further studies over a much broader range of grafting densities and molecular weights are necessary to completely understand how grafted polymers

influence NP diffusion in both unentangled and entangled polymer melts.

#### IV. CONCLUSION

Using RBS, we measure the diffusion coefficient of PMMA-grafted NPs of varying grafted molecular weight ( $N$ ) and grafting density ( $\sigma$ ) in PMMA melts of varying molecular weight ( $P$ ). These NPs diffuse  $\sim 100$  times slower than predicted according to the Stokes Einstein relation assuming a viscosity equal to bulk PMMA and a hydrodynamic NP diameter equal to the NP core. We show that this slow NP diffusion is the result of a significantly increased effective NP size  $2R_{\text{eff}} \approx 20$  nm, which is essentially independent of the grafting densities and matrix molecular weights studied. Comparing these experimental results to a modified Daoud-Cotton scaling estimate for the brush thickness and detailed dynamic mean field simulations of polymer-grafted NPs in athermal polymer melts, we find that  $2R_{\text{eff}}$  is comparable to the size of the NP core plus the extended grafted chains ( $2r_{\text{max}}$ ). Our results suggest that grafted polymer chains of moderate molecular weight and grafting density alter the NP diffusion mechanism in polymer melts, namely, by substantially increasing the NP effective size.

#### SUPPLEMENTARY MATERIAL

See the [supplementary material](#) for a comparison of the grafted polymer volume fraction profiles as determined by 3D dynamic mean field theory and 2D self-consistent field theory.

#### ACKNOWLEDGMENTS

This work was primarily funded by the National Science Foundation NSF/EPSRC Materials World Network Nos. DMR-1210379 (C.C.L., K.I.W., and R.J.C.) and EP/5065373/1 (N.C.). Support was also provided by the No. NSF/MRSEC-DMR 11-20901 (P.J.G., K.I.W., and R.J.C.), Polymer Programs No. DMR 15-07713 (R.J.C.), Dupont Central Research and Development (R.J.C.), and the ACS/PRF Program No. 54028-ND7 (R.J.C.). H.C. and R.A.R. acknowledge funding through NSF DMR 1410246. Computational resources were provided through XSEDE allocation TG-DMR150034. We thank D. Yates for assistance with ion scattering. Valuable discussions with J. Meth and K. Schweizer are gratefully acknowledged.

<sup>1</sup>M. J. A. Hore, A. L. Frischknecht, and R. J. Composto, *ACS Macro Lett.* **1**, 115–121 (2012).

<sup>2</sup>M. J. Hore and R. J. Composto, *Macromolecules* **47**, 875–887 (2014).

<sup>3</sup>J.-M. Thomassin, M. Trifkovic, W. Alkarmo, C. Detrembleur, C. Jerome, and C. Macosko, *Macromolecules* **47**, 2149–2155 (2014).

<sup>4</sup>B. C. Kim, S. W. Park, and D. G. Lee, *Compos. Struct.* **86**, 69–77 (2008).

<sup>5</sup>E. T. Thostenson, C. Y. Li, and T. W. Chou, *Compos. Sci. Technol.* **65**, 491–516 (2005).

<sup>6</sup>L.-H. Cai, S. Panyukov, and M. Rubinstein, *Macromolecules* **44**, 7853–7863 (2011).

<sup>7</sup>M. E. Mackay, T. T. Dao, A. Tuteja, D. L. Ho, B. Van Horn, H. C. Kim, and C. J. Hawker, *Nat. Mater.* **2**, 762–766 (2003).

<sup>8</sup>A. Tuteja, P. M. Duxbury, and M. E. Mackay, *Macromolecules* **40**, 9427–9434 (2007).

<sup>9</sup>A. Tuteja, M. E. Mackay, C. J. Hawker, and B. Van Horn, *Macromolecules* **38**, 8000–8011 (2005).

- <sup>10</sup>U. Yamamoto and K. S. Schweizer, *J. Chem. Phys.* **135**, 224902 (2011).
- <sup>11</sup>C.-C. Lin, E. Parrish, and R. J. Composto, *Macromolecules* **49**, 5755–5772 (2016).
- <sup>12</sup>S. Gupta, Q. L. Zhang, T. Emrick, A. C. Balazs, and T. P. Russell, *Nat. Mater.* **5**, 229–233 (2006).
- <sup>13</sup>F. B. Wyart and P. G. de Gennes, *Eur. Phys. J. E: Soft Matter* **1**, 93–97 (2000).
- <sup>14</sup>J.-P. Hansen and I. R. McDonald, *Theory of Simple Liquids* (Academic Press, London, 1986).
- <sup>15</sup>Q. Lu and M. J. Solomon, *Phys. Rev. E* **66**, 061504 (2002).
- <sup>16</sup>U. Yamamoto and K. S. Schweizer, *J. Chem. Phys.* **139**, 064907 (2013).
- <sup>17</sup>C. A. Grabowski, B. Adhikary, and A. Mukhopadhyay, *Appl. Phys. Lett.* **94**, 021903 (2009).
- <sup>18</sup>C. A. Grabowski and A. Mukhopadhyay, *Macromolecules* **47**, 7238–7242 (2014).
- <sup>19</sup>J. T. Kalathi, U. Yamamoto, K. S. Schweizer, G. S. Grest, and S. K. Kumar, *Phys. Rev. Lett.* **112**, 108301 (2014).
- <sup>20</sup>R. Mangal, S. Srivastava, S. Narayanan, and L. A. Archer, *Langmuir* **32**, 596–603 (2016).
- <sup>21</sup>J. Choi, M. Cargnello, C. B. Murray, N. Clarke, K. I. Winey, and R. J. Composto, *ACS Macro Lett.* **4**, 952–956 (2015).
- <sup>22</sup>U. Yamamoto and K. S. Schweizer, *Macromolecules* **48**, 152–163 (2015).
- <sup>23</sup>P. J. Griffin, V. Bocharova, L. R. Middleton, R. J. Composto, N. Clarke, K. S. Schweizer, and K. I. Winey, *ACS Macro Lett.* **5**, 1141–1145 (2016).
- <sup>24</sup>C. D. Chapman, K. Lee, D. Henze, D. E. Smith, and R. M. Robertson-Anderson, *Macromolecules* **47**, 1181–1186 (2014).
- <sup>25</sup>L. H. Cai, S. Panyukov, and M. Rubinstein, *Macromolecules* **48**, 847–862 (2015).
- <sup>26</sup>M. J. A. Hore and R. J. Composto, *Macromolecules* **45**, 6078–6086 (2012).
- <sup>27</sup>D. Sunday, J. Ilavsky, and D. L. Green, *Macromolecules* **45**, 4007–4011 (2012).
- <sup>28</sup>R. C. Ferrier, Y. Huang, K. Ohno, and R. J. Composto, *Soft Matter* **12**, 2550–2556 (2016).
- <sup>29</sup>T. Hoshino, D. Murakami, Y. Tanaka, M. Takata, H. Jinnai, and A. Takahara, *Phys. Rev. E* **88**, 032602 (2013).
- <sup>30</sup>A. K. Kandar, S. Srivastava, J. K. Basu, M. K. Mukhopadhyay, S. Seifert, and S. Narayanan, *J. Chem. Phys.* **130**, 121102 (2009).
- <sup>31</sup>S. Liu, E. Senses, Y. Jiao, S. Narayanan, and P. Akcora, *ACS Macro Lett.* **5**, 569–573 (2016).
- <sup>32</sup>C. Xu, K. Ohno, V. Ladmiraal, and R. J. Composto, *Polymer* **49**, 3568–3577 (2008).
- <sup>33</sup>J. E. Mark, *Physical Properties of Polymers Handbook* (Springer, New York, 2007).
- <sup>34</sup>R. J. Composto, R. M. Walters, and J. Genzer, *Mater. Sci. Eng., R* **38**, 107–180 (2002).
- <sup>35</sup>E. Helfand, *J. Chem. Phys.* **62**, 999–1005 (1975).
- <sup>36</sup>M. C. Villet and G. H. Fredrickson, *J. Chem. Phys.* **141**, 224115 (2014).
- <sup>37</sup>J. Koski, H. Chao, and R. A. Riggleman, *J. Chem. Phys.* **139**, 244911 (2013).
- <sup>38</sup>G. H. Fredrickson and H. Orland, *J. Chem. Phys.* **140**, 084902 (2014).
- <sup>39</sup>H. Chao, J. Koski, and R. A. Riggleman, *Soft Matter* **13**, 239–249 (2017).
- <sup>40</sup>K. C. Daoulas and M. Müller, *J. Chem. Phys.* **125**, 184904 (2006).
- <sup>41</sup>B. Narayanan, V. A. Pryamitsyn, and V. Ganesan, *Macromolecules* **37**, 10180–10194 (2004).
- <sup>42</sup>M. Rubinstein and R. H. Colby, *Polymer Physics* (Oxford University Press, New York, 2003).
- <sup>43</sup>G. Batchelor, *J. Fluid Mech.* **83**, 97–117 (1977).
- <sup>44</sup>Z. Cheng, J. Zhu, P. M. Chaikin, S.-E. Phan, and W. B. Russel, *Phys. Rev. E* **65**, 041405 (2002).
- <sup>45</sup>B. J. Anderson and C. F. Zukoski, *Macromolecules* **41**, 9326–9334 (2008).
- <sup>46</sup>I. M. Krieger and T. J. Dougherty, *Trans. Soc. Rheol.* **3**, 137–152 (1959).
- <sup>47</sup>I. M. Krieger, *Adv. Colloid Interface Sci.* **3**, 111–136 (1972).
- <sup>48</sup>M. Daoud and J. Cotton, *J. Phys.* **43**, 531–538 (1982).
- <sup>49</sup>K. Ohno, T. Morinaga, S. Takeno, Y. Tsujii, and T. Fukuda, *Macromolecules* **40**, 9143–9150 (2007).
- <sup>50</sup>M. J. Hore, J. Ford, K. Ohno, R. J. Composto, and B. Hammouda, *Macromolecules* **46**, 9341–9348 (2013).
- <sup>51</sup>J. Choi, M. J. Hore, N. Clarke, K. I. Winey, and R. J. Composto, *Macromolecules* **47**, 2404–2410 (2014).